Int J Thermophys (2014) 35:2140–2149
DOI 10.1007/s10765-014-1741-y

Thermal Diffusivity, Effusivity, and Conductivity of CdMnTe Mixed Crystals

K. Strzałkowski · F. Firszt · A. Marasek

Received: 20 March 2014 / Accepted: 4 September 2014 / Published online: 24 September 2014

Abstract $Cd_{1-x}Mn_xTe$ mixed crystals belong to a class of materials called "semimagnetic semiconductor" or diluted magnetic semiconductor with the addition of magnetic ions such as Mn^{2+} implemented into the crystal structure. The crystals under investigation were grown from the melt by the high-pressure high-temperature modified Bridgman method in the range of composition $0 < x < 0.7$. Thermal properties of these compounds have been investigated by means of photopyroelectric calorimetry in both back and front detection configurations. The values of the thermal diffusivity and thermal effusivity were derived from experimental data. The thermal conductivity of the specimens was calculated from the simple theoretical dependencies between thermal parameters. The influence of the Mn concentration on the thermal properties of $Cd_{1-x}Mn_xTe$ crystals has been presented and discussed.

Keywords CdMnTe crystals · Photopyroelectric calorimetry · Thermal conductivity · Thermal diffusivity · Thermal effusivity

1 Introduction

Diluted magnetic semiconductors (DMS) are materials with magnetic ions implemented into the crystal structure. These materials are interesting because of a potential application in spintronics [1] and also optoelectronics. DMS based on mixed crystals of II–VI compounds with the manganese are very promising materials for spintronics due to unique magneto-optical properties [2]. $Cd_{1-x}Mn_xTe$ crystals [3,4] show very interesting physical properties due to a strong s, p–d exchange interaction between

K. Strzałkowski (✉) · F. Firszt · A. Marasek
Institute of Physics, Faculty of Physics, Astronomy and Informatics, Nicolaus Copernicus University, Grudziadzka 5, 87-100 Toruń, Poland
e-mail: skaroll@fizyka.umk.pl

electrons, holes, and ion Mn^{+2}-3d electrons. II–VI compounds present some crucial advantages in comparison with III–V magnetic semiconductors. In II–VI crystals, manganese is an isoelectronic atom, so *n*-type and *p*-type doping is possible. Mn^{2+} ions exhibit a relatively high solubility with many II–VI binary compounds.

Photothermal methods have been widely applied to study thermal properties of solid samples [4–10]. The major advantages of these techniques are their simplicity, high sensitivity, non-destructive character, and adaptation on experimental restrictions for theoretical requirements. Among them, a photopyroelectric method can be used for thermal investigation of solids [5]. The thermal effusivity of the solid sample can be obtained in the front configuration where the incident radiation directly illuminates a sensor. On the other hand, the PPE method in the back configuration (the sample placed onto the sensor is excited by the incident radiation) allows one to obtain the thermal-diffusivity value, which describes an ability of the material to conduct heat [10]. To ensure good thermal contact in both detection configurations, a thin layer of the coupling fluid between the sample and the pyroelectric sensor is required. It was shown that the results obtained with the BPPE technique are always underestimated due to the presence of the coupling fluid between the sample and the sensor [11,12]. The influence of the coupling fluid in pyroelectric measurements of solids becomes significant especially for high conductivity samples and at high modulation frequencies of the incident radiation.

A knowledge of the thermal properties of solid solutions is important for their applications in the construction of optoelectronic devices. Thermal parameters are unique for each material; they depend on the composition, structural characteristics, and the preparation process. The aim of this article is to describe a thermal characterization (measurement of all dynamic thermal parameters) of the investigated crystals and to discuss the influence of the composition on their thermal properties. Another goal of this article is to show that by introducing a simple experimental modification, one can minimize the undesired effect of the coupling fluid.

2 Experimental Setup and Sample Preparation

Mixed $Cd_{1-x}Mn_xTe$ crystals were obtained by the high-pressure Bridgman method with different Mn concentrations. This method allows obtaining crystal rods of about one centimeter in diameter and up to a few centimeters in length. The obtained crystal rods were cut into about 1 mm thick specimens, which were not oriented along any crystallographic plane. The plates were mechanically ground and then polished with diamond paste. The structure and the lattice constant of the measured crystalline alloys were determined with the X-ray diffraction method, which confirmed that the samples exhibited a single zinc blende crystallographic phase. The real Mn concentration was obtained from the lattice constant/composition dependence for two binary semiconductors: CdTe and MnTe. Four $Cd_{1-x}Mn_xTe$ samples were investigated in this work with x equal to 0, 0.27, 0.49, and 0.67.

The standard PPE experimental setup for both front and back measurement detection configurations was used [13]. It consisted of a 300 mW power blue diode laser ($\lambda = 405$ nm), a 0.4 mm thick $LiTaO_3$ detector, provided with CrAu electrodes, and

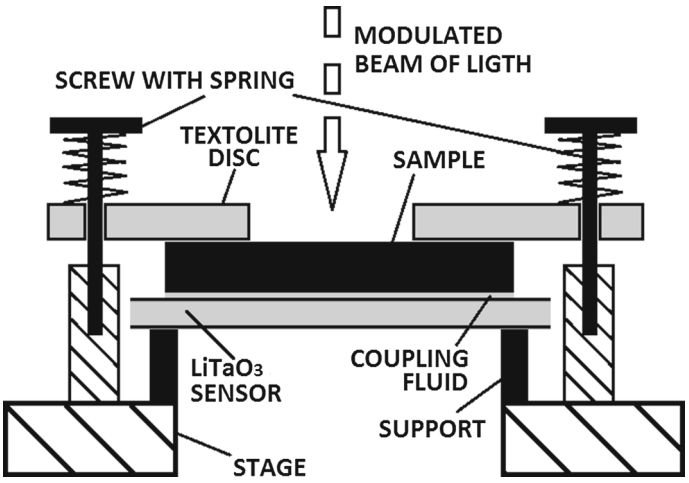

Fig. 1 Modified experimental setup for the BPPE method

a SR850 dual-phase lock-in amplifier. The reference signal provided from the internal oscillator of the lock-in was used for modulation of the incident radiation. In a standard BPPE method, the sample (placed and stuck to the sensor) is directly excited with modulated radiation, in contrast to the front mode where the sensor is being illuminated. A thin layer of ethylene glycol served as a coupling fluid between the sample and the sensor. To improve thermal contact in the back measurement configuration between the sample and the sensor, a textolite disk has been applied (Fig. 1). As a result of the springs, the disk is pressing the sample to the sensor, and at the same time preventing the detector from direct illumination. The modulation frequency of the excitation source was changed in the range of 1 Hz to 15 Hz. For both BPPE and FPPE, a configuration normalization procedure with an empty sensor was applied.

Investigated samples measured in the back configuration have been blackened with a thin carbon layer, in order: (i) to assure the optical opacity of the transparent samples and (ii) to avoid the influence of an optical exciting state of the semiconductor on its thermal properties (phonon scattering processes on free excited carriers). Because the deposited carbon layer is very thin ($<10\,\mu$m) and has a high thermal conductivity, one can neglect its influence on the signal.

All the measurements have been performed at room temperature and were computer-controlled.

3 Theory

The BPPE and FPPE cell configuration consists of four layers composed as follows: air/opaque sample/pyroelectric sensor/air (Fig. 2). Assuming perfect thermal contact between the sample and the sensor and a one-dimensional model of heat propagation through the sandwich-type system, the complex PPE signal in the back configuration is given by [13–16]

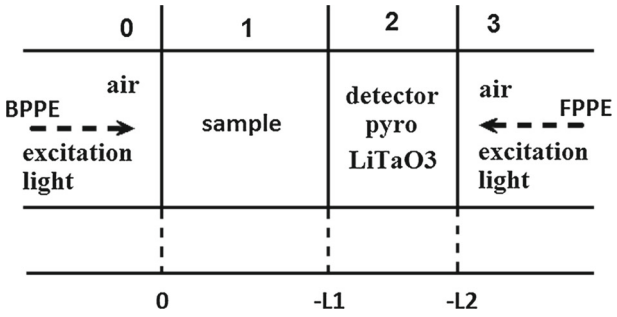

Fig. 2 Model of the experimental cell in the back and front configurations for the PPE method

$$V = \frac{2V_0 e^{-\sigma_s L_s}}{b_{sp}+1} \frac{1 - e^{-2\sigma_p L_p}}{1 + R_{sp} e^{-2\sigma_p L_p} - (R_{sp} + e^{-2\sigma_p L_p}) e^{-2\sigma_s L_s}}. \quad (1)$$

In Eq. 1, V_0 is an instrumental factor, ij represents s and p layers of the detection cell, respectively, $R_{ij} = (b_{ij} - 1)/(b_{ij} + 1)$ is the reflection coefficient of the thermal wave at the ij interface, $b_{ij} = e_i/e_j$, e is the thermal effusivity, $\sigma_i = (1 + \mathrm{i})a_i$ is the complex diffusion coefficient, a_i is the reciprocal of the thermal diffusion length μ_i, $a_i = 1/\mu_i$, $\mu_i = (2\alpha_i/\omega)^{1/2}$, ω is the angular modulation frequency, and L_i is the thickness of layer i. In order to eliminate the instrumental factor V_0, the useful signal is normalized with respect to the signal obtained with the empty sensor [13]. After the normalization procedure and assuming a thermally thick regime for both the detector and the sample ($\mu_i < L_i$), one can calculate the thermal diffusivity using the amplitude (Eq. 2) and/or the phase (Eq. 3) of the complex signal [13]:

$$\ln |V_n| = \ln \frac{2}{b_{sp}+1} - a_s L_s \quad (2)$$

$$\Theta = \Theta_0 - L_s \left(\frac{\omega}{2\alpha_s}\right)^{1/2} \quad (3)$$

The amplitude is affected by external factors such as laser-intensity fluctuations and the roughness of the surface, whereas the phase provides more accurate results, being independent of these external factors. For this reason, the thermal diffusivity was calculated according to Eq. 3, the excitation frequency being used as a scanning parameter.

In the front measurement configuration, the complex signal after normalization to the empty sensor can be written as follows [13]:

$$V_n = \frac{1 - e^{-\sigma_p L_p} + R_{sp}(e^{-2\sigma_p L_p} - e^{-\sigma_p L_p})}{1 + R_{sp} e^{-2\sigma_p L_p}}. \quad (4)$$

Equation 4 can be simplified to the following equation considering the assumption that $\mu_p \ll L_p$ (thermally thick detector):

$$V_n = 1 - (1 + R_{sp}) e^{-\sigma_p L_p}. \quad (5)$$

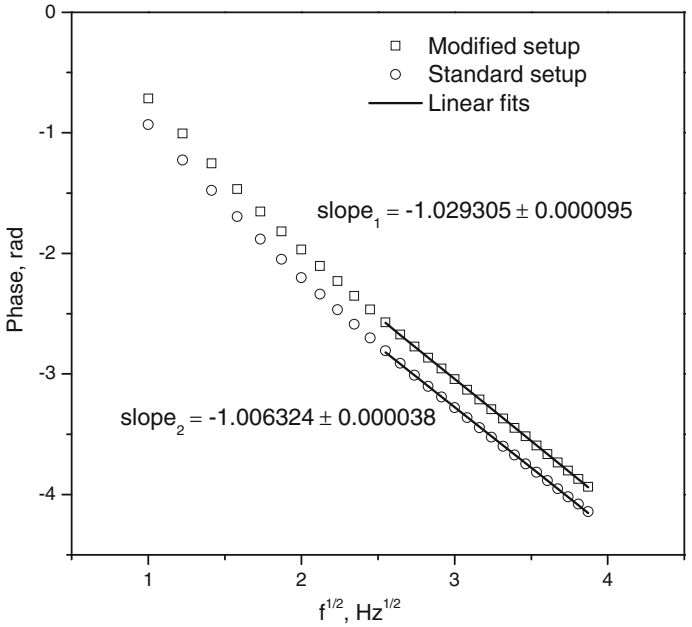

Fig. 3 Phase characteristics of the CdTe sample measured before (*squares*) and after (*circles*) the modification of the experimental setup as a function of the square root of the modulation frequency; *points* are experimental data, and *lines* are linear fits

From Eq. 5, one can get the amplitude (Eq. 6) and the phase (Eq. 7) of the signal:

$$|V_n| = \sqrt{[(1 + R_{\mathrm{sp}})\mathrm{e}^{-a_{\mathrm{p}}L_{\mathrm{p}}} \sin(a_{\mathrm{p}}L_{\mathrm{p}})]^2 + [1 - (1 + R_{\mathrm{sp}})\mathrm{e}^{-a_{\mathrm{p}}L_{\mathrm{p}}} \cos(a_{\mathrm{p}}L_{\mathrm{p}})]^2} \quad (6)$$

$$\varphi_n = \arctan \frac{(1 + R_{\mathrm{sp}})\mathrm{e}^{-a_{\mathrm{p}}L_{\mathrm{p}}} \sin(a_{\mathrm{p}}L_{\mathrm{p}})}{1 - (1 + R_{\mathrm{sp}})\mathrm{e}^{-a_{\mathrm{p}}L_{\mathrm{p}}} \cos(a_{\mathrm{p}}L_{\mathrm{p}})} \quad (7)$$

For the normalized phase (zero crossing frequency f_{o}), the following relation is true:

$$\frac{L_{\mathrm{p}}}{\mu_{\mathrm{p}}} = \pi \Rightarrow \alpha_{\mathrm{p}} = \frac{L_{\mathrm{p}}^2 f_{\mathrm{o}}}{\pi} \quad (8)$$

Equation 8 allows determination of the thermal properties of the sensor if the sample properties are known.

4 Results and Discussion

All samples investigated in this work were measured using a modified back configuration experimental setup (see Fig. 2). Phase characteristics of the CdTe sample measured before (squares) and after (circles) the modification of the experimental setup as a function of the square root of the modulation frequency are presented in Fig. 3.

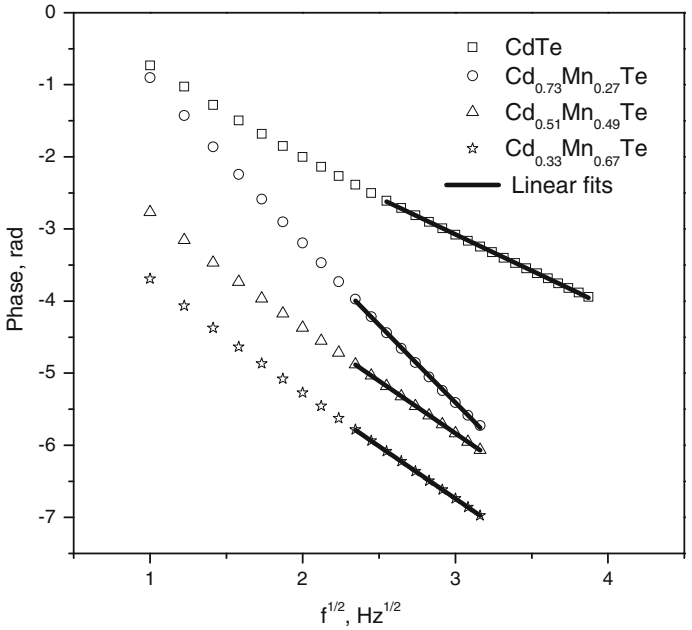

Fig. 4 PPE phases in radians of all investigated samples as a function of the square root of the modulation frequency; *points* are experimental data, and *lines* are linear fits

For the low frequency regime, a nonlinear behavior of the phase can be observed, caused by a thermally thin sample and/or the sensor. Consequently, linear fits were performed starting from 6 Hz, where both the sample and the detector are thermally thick. A least-squares method has been applied for the fitting procedure. The difference in the slopes between curves presented in Fig. 3 can be found. The thermal diffusivity of the CdTe sample was calculated according to Eq. 3 from the slopes of the fitted lines as $(4.244 \pm 0.035) \times 10^{-6}\,\mathrm{m^2{\cdot}s^{-1}}$ for a standard configuration and as $(4.473 \pm 0.008) \times 10^{-6}\,\mathrm{m^2{\cdot}s^{-1}}$ after applying the modification. The presented thermal-diffusivity values were calculated as average values from three independent measurements with the standard deviation as an uncertainty. As a result of the proposed simple solution, some reduction of the influence of the coupling fluid on the obtained thermal-diffusivity value takes place. A similar measurement procedure was applied for all mixed $Cd_{1-x}Mn_xTe$ crystals; the obtained results are displayed in Fig. 4. The thickness of the $Cd_{0.73}Mn_{0.27}Te$ sample is 1.5 times greater than that of other samples (of the order of 1.1 mm); consequently, the slope obtained for this specimen differs from the others. The thermal diffusivity of the crystals was obtained according to Eq. 3.

The thermal effusivity of the investigated materials was derived from the PPE technique in a front measurement configuration coupled with a frequency scanning procedure. For calibration and testing purposes, two well-known liquids, i.e., distilled water and ethylene glycol, were measured in the same measurement configuration as for the solid samples. Figure 5 presents phase characteristics of the investigated

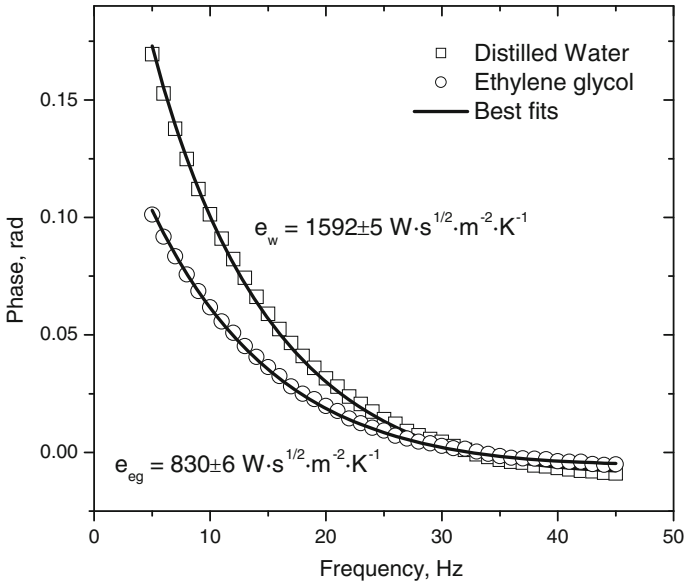

Fig. 5 Phase behavior of distilled water and ethylene glycol as a function of modulation frequency; *points* refer to measured data, and *lines* are best fits obtained with least-squares method using Eq. 7

fluids as a function of the modulation frequency, the points refer to measured data, and the lines are best fits obtained with a least-squares method using Eq. 7. The thermal-effusivity values were calculated as average values from three independent measurements with the standard deviation as an uncertainty. The obtained results for the thermal effusivity of water and ethylene glycol remain in good agreement with the literature data [17]. The phase behavior of the investigated $Cd_{1-x}Mn_xTe$ mixed crystals as a function of the modulation frequency is presented in Fig. 6 . A similar experimental procedure such as in the case of liquid samples was applied. It can be seen that all curves are crossing the zero phase point for the same modulation frequency. As a result, one can state that the measurements and normalization procedure were carried out properly. According to Eq. 8, one can use this point to obtain the thermal properties of the sensor, if necessary. Figure 7 presents phase characteristics of the CdTe crystal as a function of the modulation frequency and the error arising from the fitting procedure. The best fit of Eq. 7 obtained with a least-squares method is also displayed in Fig 7. The minimum observed in the fitting error graph corresponds to the value of the thermal effusivity of the investigated sample.

It is well known that thermal parameters are connected by simple relations. The thermal conductivity of the investigated crystals was calculated according to the following formula: $k = e\alpha^{1/2}$. Thermal parameters of all investigated specimens are presented in Table 1. Uncertainties of the thermal conductivity were calculated using the total differential method as simply average errors taking into account thermal-diffusivity and thermal-effusivity uncertainties. The calculated value of the thermal conductivity for CdTe crystals is smaller than that from the literature [18] ($6.2\,W{\cdot}m^{-1}{\cdot}K^{-1}$); however, the difference is not large. It is known that thermal parameters strongly depend

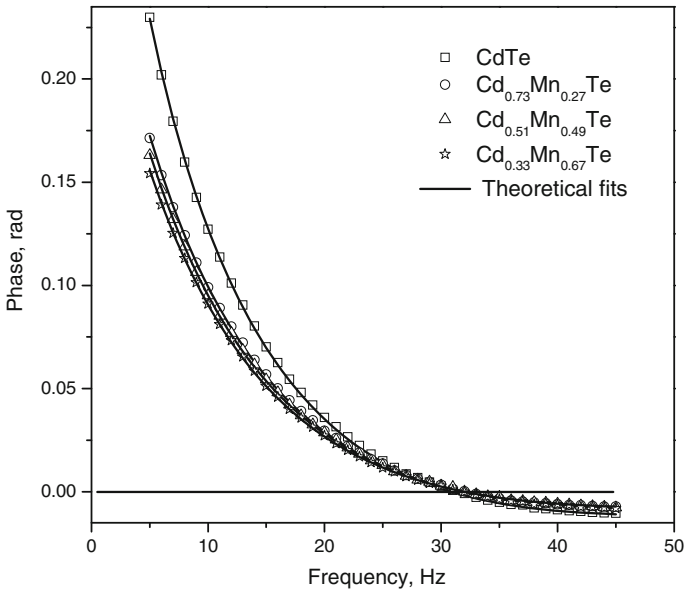

Fig. 6 Phase characteristics of mixed $Cd_{1-x}Mn_xTe$ crystals as a function of modulation frequency; *points* refer to measured data, and *lines* are best fits obtained with least-squares method using Eq. 7

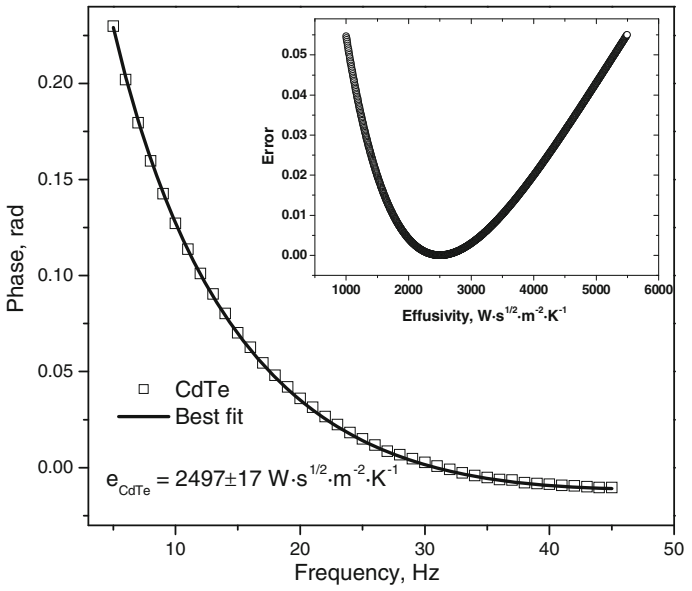

Fig. 7 Phase characteristic of CdTe crystal as a function of modulation frequency; *points* refer to measured data, *line* is best fit obtained with least-squares method using Eq. 7, and the error of the fitting procedure is displayed in *inset*

Table 1 Thermal parameters of the investigated $Cd_{1-x}Mn_xTe$ crystals

Sample	Thermal diffusivity ($10^{-6}m^2 \cdot s^{-1}$)	Thermal effusivity ($W \cdot s^{1/2} \cdot m^{-2} \cdot K^{-1}$)	Thermal conductivity ($W \cdot m^{-1} \cdot K^{-1}$)
Cdte	4.473 ± 0.008	2497 ± 17	5.280 ± 0.042
$Cd_{0.73}Mn_{0.27}Te$	1.734 ± 0.012	1592 ± 8	2.096 ± 0.017
$Cd_{0.51}Mn_{0.49}Te$	1.478 ± 0.016	1510 ± 15	1.836 ± 0.028
$Cd_{0.33}Mn_{0.67}Te$	1.418 ± 0.007	1432 ± 7	1.705 ± 0.0136

on the fabrication process and quality of the crystal structure. One can see in Table 1 that manganese incorporated into the crystal structure leads to a decrease of all the thermal parameters of the specimens. A similar behavior was observed previously for $Zn_{1-x}Mg_xSe$ and $Cd_{1-x-y}Zn_xMg_ySe$ mixed compounds [19]. In our opinion, this effect is mainly due to the difference in the atomic radius of the components and, as a consequence, the periodic potential of the crystal is perturbed. Each crystal imperfection in such a material becomes a potential scattering center for phonons and, consequently, the ability of the material to conduct the heat is reduced.

5 Conclusions

$Cd_{1-x}Mn_xTe$ mixed crystals investigated in this work were grown with the modified Bridgman method. The PPE method has been applied to determine the thermal parameters of the specimens. Measurements were performed in both back and front detection configurations. It allowed determination of the thermal-diffusivity and thermal-effusivity values, respectively. In the back PPE mode, some modification of the experimental setup was proposed, which allowed reduction of the influence of the coupling fluid on the value of the thermal diffusivity. Distilled water and ethylene glycol were measured first in the front configuration for testing the reliability of the method. The obtained thermal-effusivity values of the liquid samples were consistent with the literature data. The thermal conductivity of the investigated specimens was calculated from the relations between thermal parameters. An uncertainty of the thermal parameters was estimated as of the order of 1 %. The experimental results demonstrated that an increase in the content of manganese leads to a decrease in the values of all thermal parameters.

References

1. R. Fitzgerald, Phys. Today **53**, 21 (2000)
2. G. Theurich, N.A. Hill, Phys. Rev. B **66**, 115208 (2002)

3. J. Zakrzewski, F. Firszt, S. Łęgowski, H. Męczyńska, M. Pawlak, A. Marasek, Rev. Sci. Instrum. **74**, 566 (2003)
4. J. Zakrzewski, F. Firszt, S. Łęgowski, H. Męczyńska, A. Marasek, M. Pawlak, Rev. Sci. Instrum. **74**, 572 (2003)
5. D. Dadarlat, J. Therm. Anal. Calorim. **110**, 27 (2012)
6. D. Trefon-Radziejewska, J. Bodzenta, A. Kaźmierczak-Bałata, T. Łukasiewicz, Int. J. Thermophys. **33**, 707 (2012)
7. M. Pawlak, M. Maliński, F. Firszt, J. Pelzl, A. Ludwig, A. Marasek, Meas. Sci. Technol. **25**, 035204 (2014)
8. A. Kaźmierczak-Bałata, J. Bodzenta, D. Trefon-Radziejewska, Int. J. Thermophys. **31**, 180 (2010)
9. D. Trefon-Radziejewska, J. Bodzenta, T. Łukasiewicz, Int. J. Thermophys. **34**, 813 (2012)
10. M. Pawlak, M. Maliński, Infrared Phys. Technol. **64**, 87 (2014)
11. A. Salazar, A. Oleaga, Int. J. Thermophys. **33**, 1901 (2012)
12. A. Salazar, A. Oleaga, Rev. Sci. Instrum. **83**, 014903 (2012)
13. D. Dadarlat, Laser Phys. **19**, 1330 (2009)
14. M. Chirtoc, G. Mihailescu, Phys. Rev. B **40**, 9606 (1989)
15. A. Mandelis, M.M. Zver, J. Appl. Phys. **57**, 4421 (1985)
16. M. Chirtoc, C. Glorieux, J. Thoen, Thermophysical Properties and Critical Phenomena Studied by the Photopyroelectric (PPE) Method, in *Thermal Wave Physics and Related Photothermal Techniques: Basic Principles and Recent Developments*, ed. by E.M. Moares (Transworld Research Network, Trivandrum, Kerala, 2009), pp. 125–158
17. J.A. Balderas-Lopez, A. Mandelis, Int. J. Thermophys. **24**, 463 (2003)
18. http://www.crystran.co.uk/optical-materials/cadmium-telluride-cdte/. Accessed 17 March 2014
19. K. Strzałkowski, Mater. Sci. Eng. B **184**, 80 (2014)